IJE TRANSACTIONS A: Basics Vol. 25, No. 4, (October 2012) 333-346

International Journal of Engineering

Journal Homepage: www.ije.ir

Parametric Study of the Covering Soil of Tunnels Constructed in Liquefiable Soil

S. M. Marandi*, A .R. Rasti

Department of Civil Engineering, Shahid Bahonar University, Kerman, Iran

PAPER INFO

Paper history:
Received 31 May 2012
Received in revised form 5 August 2012
Accepted 30 August 2012

Keywords:
Liquefaction
Tunnel
Water Bulk Modulus
Porosity
Groundwater Level

ABSTRACT

Earthquake and its catastrophic failures is one of the disturbance worry of Civil Engineers. In geotechnical science, liquefaction is one of the most important phenomenon induced by earthquake. A change in pore water pressure follows a change in effective stress, and in a critical state in which pore-water pressure equals the total stress in soil particles, soil strength is suddenly lost and liquefaction occurs. This phenomenon causes destruction of structures constructed above ground surface or underground. In case of constructing underground structures or passing a tunnel through weak or compressible soils, with increase in forces and moments surrounding the structures leading to liquefaction, may impose damages to adjacent structures or soils. In this paper, a tunnel passing through a soil media with liquefaction potential is modeled. After static equilibrium, dynamic analyses are performed. Using liquefaction modeling and measurement of induced forces and moments of covering soil of the tunnel, parameters such as water bulk modulus, groundwater level, and porosity are investigated. The results showed that the above mentioned parameters have considerable effects on variation of effective stresses, induced forces, moments and surface dilation of the covering soil of the tunnel.

doi: *10.5829/idosi.ije.2012.25.04a.05*

1. INTRODUCTION[1]

Liquefaction is an important phenomenon in geotechnical engineering considered by many researchers. A change in pore-water pressure follows a change in effective stress, and in a critical state in which pore-water pressure equals the total stress in soil particles, soil strength is suddenly lost and liquefaction occurs. There are three main superstructure and underground structure destructions and settlements caused by soil liquefaction.

Many researches are conducted on superstructure destructions caused by liquefaction which are usually observed by settlements [1- 7]. In some parts of the world, large destructions induced by liquefaction have been reported. For example in 21st September 1999 Taiwan Chi-Chi earthquake, many structures such as: roads, bridges and buildings damaged, leaned or overturned [8]. In this disaster, number of infrastructures were also severely damaged. In 1990, in Manjil and its suburb areas earthquake in Iran, some destructions were reported [9]. Other earthquakes leading to liquefaction which could be mentioned are Niigata [10], Nihonkai-Chubu [11], Kushiro-Oki [12], and Hokkaido Nansie-Oki earthquake [13].

Destruction of the main roads was observed first in Niigata (1964), followed by Alaska earthquakes [14]. Afterward, earthquake effects on infrastructures was concerned by many researchers [15- 19].

In Kube earthquake (1995), the imposed damages to the Daikai station were reported as a subsurface structure [20]. Other underground structure destructions to be mentioned are severe damages imposed on mountain tunnels by Taiwan earthquake, in city centre and destructions of Duze earthquake in Turkey [21]. In this earthquake, highway tunnels severely damaged. There are other reports on destruction of large underground structures by earthquakes such as Tangshan in China [22], and Loma Preita in U.S.A [23].

Although limited reports exists from large underground destructions caused by soil liquefaction, but due to the fast development in cities and construction of large structures such as underground metros built in underground with liquefaction potential during earthquake, investigation on this subject is inevitable [24]. Chou et al. investigated on damages raised on shield tunnels caused by liquefaction [25].

* *Corresponding Author Email: marandi@uk.ac.ir*, Tel: +98-341-2442947, Mobile: +98-913-1404195 (S. M. Marandi)

Khoshnoudian, 1999 worked on seismic behavior of tunnels constructed in liquefiable soils in his PhD program [26]. Khoshnoudian and Shahrour, 2002 carried out a numerical research on the seismic behavior of tunnels constructed in liquefiable soils [27]. In their research, they investigated a rectangular station for the effects of loading frequency, loading amplitude, permeability, and dilation angle using finite element method and Dyna Swandy software. Liu and Song, worked on seismic response of large underground structures in liquefiable soils subjected to horizontal and vertical earthquake excitations [28, 29].

They investigated on forces resulting from liquefaction with variation in parameters such as: lateral deformation and underground structure internal forces, vertical loading, and embedment depth on tunnel. In a PhD thesis, Azadi, 2008 worked on the effects of parameters such as: internal soil friction, tunnel diameter, embedment depth of tunnel, releasing coefficient, loading frequency, loading amplitude, and vertical seismic forces on underground structures [30]. Azadi and Mir Mohammad Hoessini carried out researches on the effects of seismic behavior of shallow tunnels in liquefiable grounds under cyclic loadings [31, 32]. For their analysis, they used a soil with porosity of 0.30 and unit weight of 1500 kg/m^3. Tokida and Ninomiya performed an experimental study on the uplift deformation of underground structures induced by soil liquefaction [33]. They placed an aluminum quadratic tunnel in a soil with liquefaction potential using vibration table. Bulk modulus of water is also an important parameter that varies due to geographical and weather conditions. Bahadori and Hari worked on various bulk moduli of marine and fresh waters [34]. They found that bulk modulus water varies with variation in water hardness.

A review of the literature regarding to parameters affective on underground structures placed in ground with liquefaction potential shows that there have been considerable theoretical and practical studies in this respect. Despite all the various researches undertaken on this issue, the authors of this article did not find new researches carried out on the effects of bulk modulus of water, underground water level, and soil coefficient of porosity on underground structures built in ground with liquefaction potential. Thus, new study results may be fruitful for analysis of underground structures such as: tunnels, buried pipes, and any structures of these types at risk of earthquake in ground with liquefaction potential. In addition, the new findings may be helpful in understanding the behavior of covering soils on these structures especially in engineering projects in which these types of constructions are used. The main objectives of this research is dynamic analysis and determination of the effects of liquefaction on covering soil of a tunnel built in underground while the parameters of water bulk modulus, underground water level, and coefficient of the soil porosity are changing.

2. MODELING

A saturated sand layer with liquefaction potential is modeled and equilibrated at static loading. A tunnel is excavated in the model and is equilibrated again with static loading. Then, with application of dynamic loading, the effect of liquefaction on underground structure and variation of various parameters of covering soil of the tunnel is investigated. For modeling of soil-tunnel, FLAC software and a model net of $30m \times 50m$ with length of $1m$ is used. The specification and dimension of the model and network are shown in Table 1 and Figure 1, respectively. Two specificifications of the general fluid formulation require attention:

1. The fluid equations and boundary conditions in FLAC are expressed in terms of pressure rather than head, although the latter is more common in soil mechanics.

2. The "permeability" used in FLAC is the mobility coefficient: the coefficient of the pore pressure term in Darcy's law. It is defined as the ratio of intrinsic permeability to fluid dynamic viscosity [35].

The soil used in model was Nevada sand and for soil modeling, Finn model is used. The Finn model provided with FLAC for simulating liquefaction uses Mohr-Coulomb failure criteria along with an assumed linear elastic-perfectly plastic stress-strain behavior.

The linear elastic behavior is governed by the bulk and shear moduli which can be decreased through the analysis by the user to encounter losses of soil stiffness during liquefaction. Pore-water pressure generation is modeled by computing volumetric strains induced by the cyclic shear strains using a formulation given by Martin et al. [35]. In this formulation, the volumetric strain increment ($\Delta\varepsilon v$) occurring in any cycle of loading depends on the shear strain (γ) which occurs during that cycle as well as the previously accumulated volumetric strains (εv):

$$\Delta\varepsilon v = C_1 \exp(-C_2 \cdot \varepsilon v/\gamma) \quad (1)$$

where in Equation (1), $\Delta\varepsilon v$ = volumetric strain increment that occurs over the current cycle, εv=accumulated volumetric strains occurred over the previous cycles, γ = amplitude of the shear strain for the current cycle, and C_1 and C_2= constants dependent on the volumetric strain behavior of the sand and are calculated as follows:

$$C_1 = 7600(D_r)^{-2.5} = 8.7(N_1)_{60}^{-1.25} \quad (2)$$

$$C_2 = 0.4/C_1 \quad (3)$$

TABLE 2. Specifications of protector structure

Tunnel diameter (*m*)	Covering tunnel thickness (*m*)	Modulus of elasticity (*GPa*)	Concrete unit weight (*kN/m³*)
6.9	0.3	2.236×10^{10}	24

TABLE 3. Specifications of intermediate elements

Shear hardness (K_s) (*MPa*)	Vertical hardness (K_n) (*MPa*)	Internal friction (δ) (*Degree*)
63	63	15

where in Equations (2) and (3), D_r is the relative density of the soil and $(N1)_{60}$ is the corrected blows in standard penetration test.

In order to verify the numerical model, Koohi modeled and analyzed numerically the first centrifuge model test of Verification of Liquefaction Analysis by Centrifuge Studies (VELACS). Results of this analysis [36] proved that the Finn Model adopted in the FLAC Computer Code is able to model properly liquefaction and lateral spreading phenomena [37].

Martin and Finn (1975) worked on fundamentals of liquefaction under cyclic loading [38]. They presented Equation (4) for variation of volume strain increase and cyclic shear strain. In this equation, with equating shear strain, γ to zero, the volume strain $\Delta\varepsilon_{vd}$ will be zero. Thus, Equation (5) can be used for correlation between the coefficients.

$$\Delta\varepsilon_{vd} = C_1(\gamma - C_2\varepsilon_{vd}) + \frac{C_3\varepsilon_{vd}^2}{\gamma + C_4\varepsilon_{vd}} \quad (4)$$

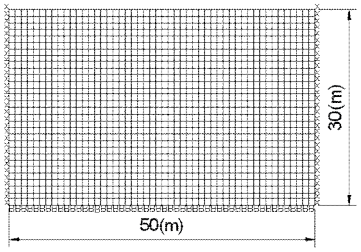

Figure 1. Model dimension and network

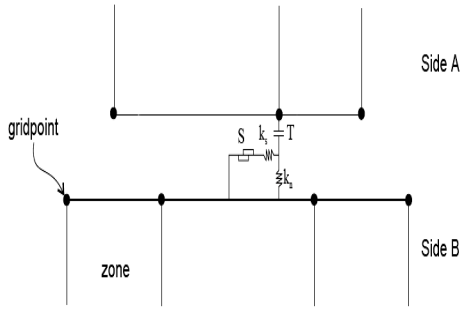

Figure 2. Schematic diagram of intermediate elements [35]

TABLE 1. Specification of the soil model

Soil Type	Sand
Behavior Model	Finn
Shearing Modulus (G)	20 (*MPa*)
Bulk Modulus (B)	30 (*MPa*)
Porosity (n)	0.3
Internal Friction (φ)	20 (Degree)
Cohesion (c)	0 (*kPa*)
Dry Unit Weight (γ_d)	15 (kN/m^3)
Tensile Strength (σ_t)	0 (*MPa*)
C_1	0.76
C_2	0.52
C_3	0.20
C_4	0.50

In Equation (4), C_1, C_2, C_3, and C_4 are determined from cyclic tri-axial tests and the following relations:

$$C_1C_2C_4 = C_3 \quad (5)$$

where, C_1 and C_2 are determined as follows:

$$C_1 = 7600(Dr)^{-2.5} \quad (6)$$

where, D_r is relative density of the soil and can be determined based on experimental Equation (7) in respect to standard penetration number, N_1 as follows:

$$Dr = 15(N_1)_{60}^{0.5} \quad (7)$$

with combination of the Equations (6), and (7), the following relation is derived:

$$C_1 = 8.7(N_1)_{60}^{-1.25} \quad (8)$$

$$C_2 = \frac{0.4}{C_1} \quad (9)$$

Damper used in model was local damper with coefficient of 5%. For modeling of tunnel and intermediate elements, the specifications presented in Tables 2, and 3 are used. Figure 2 shows schematic diagram of intermediate elements between tunnel and

soil which were selected using Linker springs. Shear and vertical hardness which are important parameters used for intermediate element definition are determined using Equation (10).

$$K_n \& K_s = \max[\frac{K + \frac{4}{3}G}{\Delta Z_{\min}}] \quad (10)$$

where, s is slider, K_n and K_s are normal and shear hardness respectively, and K, G, and $\Delta Z_{\min}$ are bulk modulus, shear modulus, and minimum width of the zones close to intermediate element, respectively. Boundary condition for dynamic case is free-field condition. The seismic input is normally represented by plane waves propagating upward through the underlying material. The boundary conditions at the sides of the model must account for the free-field motion which would exist in the absence of the structure. In some cases, elementary lateral boundaries may be sufficient. These boundaries should be placed at sufficient distances to minimize wave reflections and achieve free-field conditions. For soils with high material damping, this condition can be obtained with a relatively small distance [38]. However, when the material damping is low, the required distance may lead to an impractical model. An alternative procedure is to "enforce" the free-field motion in such a way that boundaries retain their non-reflecting properties- i.e., outward waves originating from the structure are properly absorbed. This approach used in the continuum finite-difference code NESSI [39]. A technique of this type developed for *FLAC*, involving the execution of a one-dimensional free-field calculation in parallel with the main-grid analysis. The unbalanced forces from the free-field grid are applied to the main-grid boundary. Both conditions are expressed in Equations (11) and (12), which apply to the left-hand boundary. Similar expressions may be written for the right-hand boundary:

$$F_x = -\left[\rho C_p \left(v_x^m - v_{xx}^{ff}\right)\right]\Delta S_y \quad (11)$$

$$F_y = -\left[\rho C_s \left(v_y^m - v_{xy}^{ff}\right)\right]\Delta S_y \quad (12)$$

where in Equations (11) and (12), ρ = density of material along vertical model boundary, C_p = p-wave speed at the left-hand boundary, C_s = s-wave speed at the left-hand boundary, ΔS_y = mean vertical zone size at boundary grid-point, v_x^m = x-velocity of grid-point in main grid at left boundary, v_{xx}^{ff} = x-velocity of grid-point in left free field, v_y^m = y-velocity of grid-point in main grid at left boundary, and v_{xy}^{ff} = y-velocity of grid-point in left free field. In this way, plane waves propagating upward suffer no distortion at the boundary due to the free field grid supplies conditions that are identical to those in an infinite model [35].

For loading, a sinus wave with $1HZ$ and $0.1g$ amplitude applied downward is used. The latter is close to fundamental frequency of homogenous soil mass having the mean value of the initial elastic modules of the references case ($f_1 = 0.75\,Hz$) [27]. Water table is assumed to be at ground level.

2. 1. Model Calibration For calibration, the base model shown in Figure 3 is used.

Figures 4 and 5 show the effective stress and pore-water pressure against time for base model at $19m$ depth. The results indicate that the liquefaction starts when effective stress reaches to zero. This result are in agreements with findings of Azadi, 2008 [30]. For comparison between new model and previous ones presented by other researchers, at depth $19m$ below the tunnel the results agreed with the ones obtained by others, where at this point, liquefaction occurs for both base model and previous models. For more investigation, at $5m$ depth above the base model, the results were compared. Due to the lack of laboratory or numerical results in hand for other parameters, the results compared with the base model which was calibrated and compared with previous models.

2. 2. Calculation of Water Bulk Modulus Bulk modulus of materials measures the strength at uniform pressure. One of the parameters that has quick and precise role in flow analysis is the water bulk modulus. When selected improperly, analysis are not precise without reasons or analysis period increase considerably. Thus, proper selection of this parameter can be effective in flow analysis and can be defined from Equation (13).

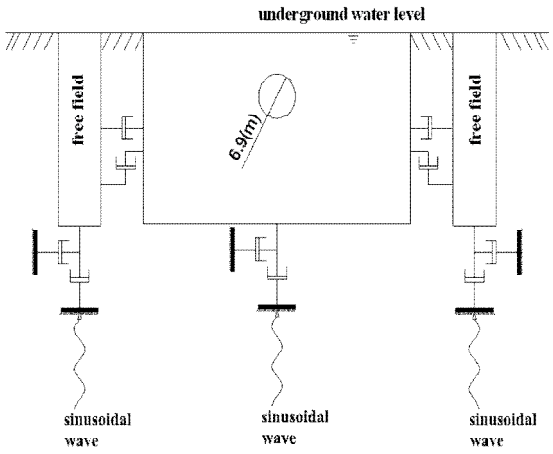

Figure 3. Base model sample [28]

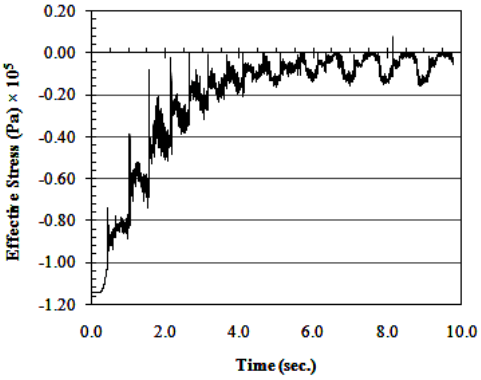

Figure 4. Effective stress versus time (for base model at 19*m* depth)

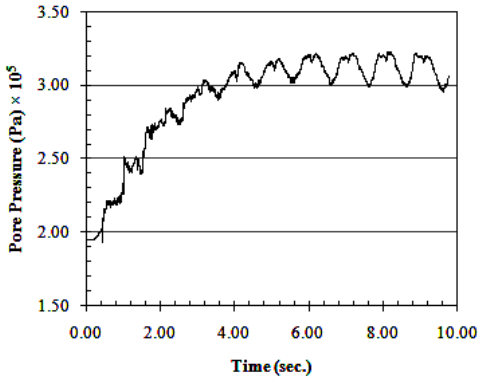

Figure 5. Pore pressure versus time (for base model at 19*m* depth)

$$K_w = -\frac{\Delta P}{\Delta V/V} \quad (13)$$

where, ΔP is variation in pressure and $\Delta V/V$ is volume strain ratio. Since determination of water bulk modulus from Equation (7) is difficult, the maximum amount of this parameter is usually used as an actual amount. The maximum suggested amount for water bulk modulus is 2 *GPa* [35]. Since this amount is generally derives from bulk and shear modulus of soil and is very higher than its equivalent amount K+4/3G, convergence is very low and analysis period increase considerably. So, water bulk modulus must be decreased as much as possible. A minimum amount for water bulk modulus is presented in FLAC software. This amount is calculated from Equation (14).

$$K_w > aL_z\rho_w g \quad (14)$$

where, a is a factor and is suggested to be 0.30 [35], and L_z is the minimum length of the zone. The amount of water bulk modulus must be selected from limitations presented in Equation (15) and close to K+4/3G to minimize the time analysis and increase in exactness of the results [29]. In the present work, the amount of water bulk modulus is assumed to be 30*MPa*.

$$aL_z\rho_w g < K_w < 2GPa \quad (15)$$

Bahadori and Hari, 2009 carried out a laboratory study and calculated various water bulk modulus [34]. In this research they found that water bulk modulus varies with weather and environmental conditions. Their findings are tabulated for sea and fresh waters at various pressures and temperatures (see Table 4).

Based on Equation (15), water bulk modulus used in FLAG software must be selected in limitation of 2×10^4 *Pa* to 2×10^9 *Pa*. In the present work, models with water bulk modulus of 3×10^4, 3×10^5, 3×10^6, and 3×10^7 are selected and their effects on liquefaction and various parameters of soil-tunnel are analyzed.

TABLE 4. Variation in water bulk modulus [33]

Temperature (°C)	Pressure (*kPa*)	Liquid type	Calculated fresh water bulk modulus (*kPa*)	Fresh water bulk modulus (reported data) (*kPa*)	Average absolute deviation percent (%)
10	100	Fresh water	2,098,400	2,100,000	0.080
25	5000	Fresh water	2,242,200	2,240,000	0.098
40	10,000	Fresh water	2,318,500	2,320,000	0.065
50	20,000	Fresh water	2,381,800	2,380,000	0.076
10	45,000	Fresh water	2,351,900	2,350,000	0.080
٠,٠	55,000	Fresh water	2,284,000	2,285,000	0.043
40	10,000	Sea water	2,471,700	2,470,000	0.069
30	20,000	Sea water	2,508,600	2,510,000	0.056
20	35,000	Sea water	2,552,200	2,555,000	0.110
10	45,000	Sea water	2,541,900	2,540,000	0.075
٠,٠	55,000	Sea water	2,503,900	2,500,000	0.156

2. 2. 1. Water Bulk Modulus Effect on Pore-water Pressure Figures 6 and 7 show the variation of pore-water pressure against time for 5*m* and 19*m* depths, respectively. The results indicate that at a constant time, with increase in water bulk modulus, pore-water pressure increase for both depths, however pore-water pressure increases with increase in water bulk modulus. For water bulk modulus variation of 3×10^4 to 3×10^6, pore-water pressure increases with moderate slope at the beginning and then increase with time with steeper slope. While, for water bulk modulus more than 3×10^6 pore-water pressure reach to a maximum point and then drop to a constant value.

For sample with water bulk modulus of 3×10^7, pore-water pressure reaches to its maximum value at first second and for sample with water bulk modulus of 3×10^8 it occurs in the first four seconds. Increasing slopes for samples with water bulk modulus of 3×10^4, 3×10^5 and 3×10^6, are 0.2%, 2%, and 9.6%, respectively. While for sample with water bulk modulus of 3×10^8, the slope reaches to its maximum value of 47%.

The results also show that for increase of water bulk modulus to 3×10^8, pore-water pressure increases in the first three seconds and then drop to lower values. Similar trend is observed for variation of pore-water pressure for 19*m* depth. With increase in water bulk modulus, the dynamic loading effect on model increases in such a way that, in sample with bulk modulus of 3×10^8 the square elements deform after 4^{th} seconds and liquefaction occurrence at various points cause destruction of the geometry of the model. Following this phenomenon and at 19*m* depth, pore-water pressure in sample with bulk modulus of 3×10^8 decreases in comparison with the sample with bulk modulus of 3×10^7. However, at a constant time, the pore-water pressure at 19*m* depth is quite higher than 5*m* depth. This can be due to the differences exist in the relative densities which increase with depth.

2. 2. 2. Water Bulk Modulus Effect on Effective Stress Effective stress is generally affected by water bulk modulus and pore-water pressure. The variation of effective stress against time for 5*m* and 19*m* depths are shown in Figures 8, and 9. Variation of pore-water pressure in models with water bulk modulus less than 3×10^6 *Pa* is not noticeable in comparison with total stress. Thus, decrease in effective stress is not considerable. Increase in water bulk modulus to more than 3×10^6 *Pa* causes decrease in effective stress and occurrence of liquefaction phenomenon. As shown in Figure 8, the model with water bulk modulus of 3×10^8 *Pa* the effective stress reaches to zero and consequently liquefaction occurs. In Figure 9, variation of effective stress with time for 19*m* depth shows similar behavior. In this regard, for models with water bulk modulus less than 3×10^6 *Pa*, variation of effective stress is not noticeable. With increase in water bulk modulus to 3×10^7 *Pa*, effective stress decreases and causes liquefaction. However, with greater water bulk modulus and due to the weight of surcharge layers, the effective stress does not lead to zero and liquefaction is not predicted. Thus, in the model with water bulk modulus of 3×10^8 *Pa*, and at 19*m* depth, the liquefaction is not occurred. However, in the same model and due to liquefaction occurrence for other depths, the geometry of the model deform and effective stress for some points decrease while, the liquefaction phenomenon is observed at more points in comparison with other models.

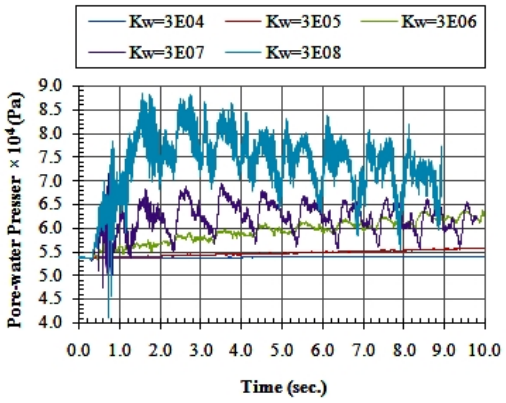

Figure 6. Pore pressure versus time (at 5*m* depth for variation in water bulk modulus)

2. 2. 3. Water Bulk Modulus Effect on Surface Dilation in the Middle of the Model Variation in water bulk modulus is also effective on the surface dilation in the middle of the model. Figure 10 shows the variation of the surface dilation with time for samples with variation in water bulk modulus. The results indicate that the variation of surface dilation in the middle of the model has an increasing rate and does not lead to a constant rate. However, variation in water bulk modulus to 3×10^6 *Pa*, causes increase in surface dilation of less than 17*cm*. The surface dilation in the model with water bulk modulus to 3×10^7 *Pa* is due to the tunnel uplift forces caused by liquefaction, and reaches to its maximum value of 40 *cm*. As explained in section 2.2.2, increase in water bulk modulus to more than 3×10^8 *Pa*, does not cause liquefaction. Besides, the minimum surface dilation shown in Figure 10 is almost 10*cm*.

2. 2. 4. Water Bulk Modulus Affects on Axial and Shear Forces and Bending Moment Variation of maximum bending moment in the covering soil of the tunnel against time for various water bulk modules is shown in Figure 11. The results show that with increase in water bulk modulus up to $3\times10^{6}\,Pa$ with time the bending moment increases up to 3 seconds and then reaches to a constant value. While, for water bulk modulus more than $3\times10^{6}\,Pa$ and cases where water bulk modulus is between $3\times10^{7}\,Pa$ and $3\times10^{8}\,Pa$, the bending moment increases up to 3 seconds and then decrease considerably in such a way that the maximum bending moment for the sample with water bulk modulus of $3\times10^{8}\,Pa$ at 9 seconds decrease to less than $7\times10^{4}\,Pa-m$.

Figure 12 shows the variation of maximum shearing forces of the covering soil of the tunnel against time for various water bulk modules. The results show that for all cases the maximum shearing forces are negative and reach to its maximum value $\left|-10\times10^{4}\right|pa$ at 3 seconds.

In cases where water bulk modulus is less than $3\times10^{6}\,Pa$ a considerable variation in shearing force is not observed. For water bulk modulus of $3\times10^{7}\,Pa$, similar to previous cases the maximum shearing force reaches to its maximum value at third seconds, but beyond this time and in contrast with previous models, the shearing forces decrease and reach to less than $\left|-8\times10^{4}\right|Pa$ at 9 seconds. This trend is observed for higher values of water bulk modulus in such a way that the maximum shearing force at 9 seconds reaches to less than $\left|-6\times10^{4}\right|Pa$. Variation in maximum axial forces in the covering soil of the tunnel against time for various water bulk modules is shown in Figure 13. The results show that for all cases the maximum axial force reaches to its maximum value of $73\times10^{4}\,Pa$ between 2 and 3 seconds. For cases where the water bulk modulus is less than $3\times10^{6}\,Pa$ with increase in water bulk modulus, considerable variation in axial forces is not observed and has steady value of $73\times10^{4}\,Pa$ up to final seconds. Similar to previous cases where the water bulk modulus is $3\times10^{7}\,Pa$ the axial force reaches to its maximum value between 2 and 3 seconds.

However, beyond 3 seconds, its magnitude decreases and reaches to less than $67\times10^{4}\,Pa$ at 10^{th} second which is in contrast with previous models. With increase in water bulk modulus similar trend is observed. For water bulk modulus of $3\times10^{8}\,Pa$ the maximum shearing force reaches to less than $65\times10^{4}\,Pa$ at 9^{th} second.

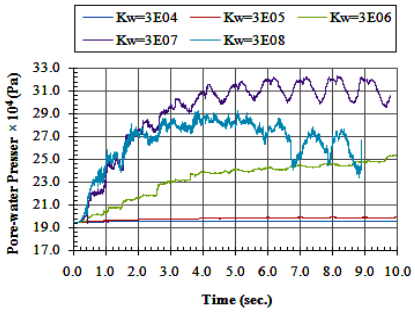

Figure ۷. Pore pressure versus time (at 19m depth for variation in water bulk modulus)

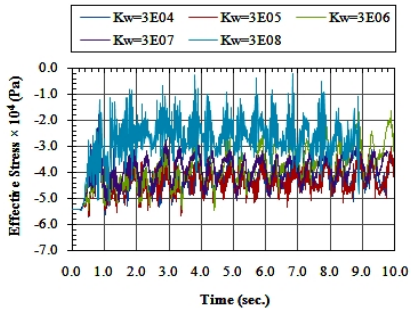

Figure 8. Effective stress versus time (at 5m depth for variation in water bulk modulus)

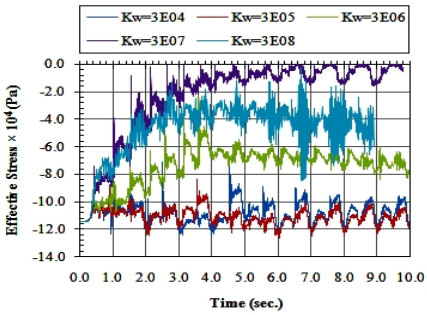

Figure 9. Effective stress versus time (at 19m depth for variation in water bulk modulus)

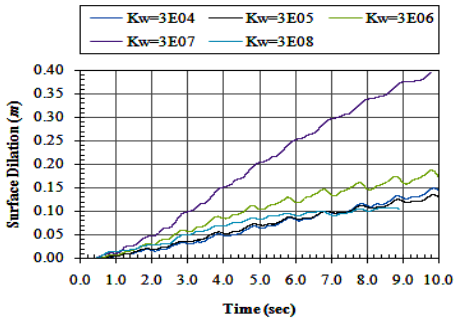

Figure 10. The surface dilation versus time (for variation in water bulk modulus)

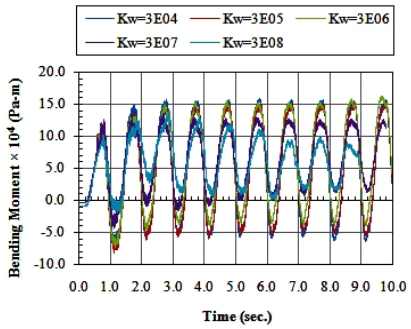

Figure 11. The bending moment versus time (for variation in water bulk modulus)

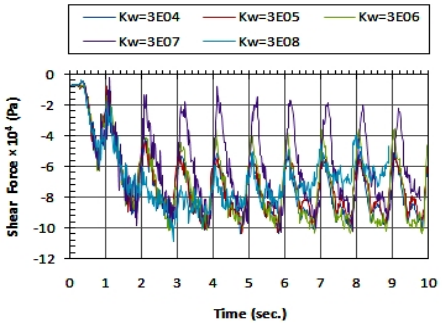

Figure 12. Shear force versus time (for variation in water bulk modulus)

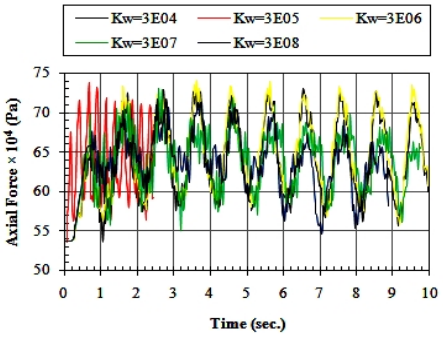

Figure 13. Axial force versus time (for variation in water bulk modulus)

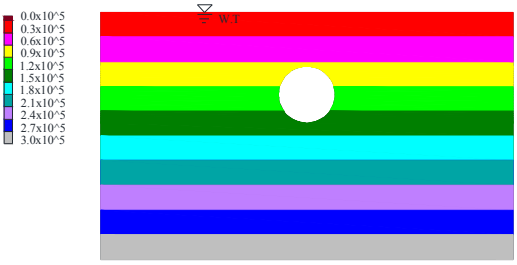

Figure 14. Pore-water pressure contour lines (for underground water level at ground surface)

2. 3. The Effect of Underground Water Level on Creation of Liquefaction and Forces in the Covering Soil of the Tunnel Since liquefaction occurs in saturated soils, underground water level is an affective parameter in creation of liquefaction and forces in the covering soil of the tunnel.

Figures 14 and 15 show pore water pressure contour lines for cases where underground water level is at ground surface and in 6*m* depth, respectively. Figure 15 shows that for underground water level above 6*m* pore-water pressure is zero and is shown by red contour lines.

2. 3. 1. The Effect of Groundwater Level on Pore Water Pressure Variations in pore-water pressure against time at depths of 5*m* and 19*m* for various groundwater levels are shown in Figures 16 and 17. Results show that at a constant time with decrease in groundwater level pore-water pressure decreases. Dynamic load causes increase in pore-water pressure with time at both depths of 5*m* and 19*m*. This trend continues up to 3 seconds and then changes to steady state. It is also noticed that the pore-water pressure values are different for 5*m* and 19*m* depths in such a way that in Figure 16 pore-water pressure is zero beyond 6*m* depth, while for 19*m* depth in Figure 17 the magnitude of pore-water pressure is considerable.

2. 3. 2. The Effect of Groundwater Level on Effective Stress Decrease in groundwater level affects on pore-water pressure and creation of stresses in covering soil of the tunnel. Figure 18 shows the variation of effective stress against time for models with various groundwater levels at 5*m* depth. Based on groundwater levels the variation curves for depths 0-6*m* are effective stresses and for other depths are total stresses against time. At depths above the tunnel, the effect of variation of weights due to unsaturated soil is not considerable and lowering groundwater level causes decrease in effective stress. Figure 19 shows the variation of effective stress against time at 19*m* depth. With lowering groundwater level, the decrease in magnitude of pore-water pressure is effective in decreasing liquefaction potential. The results also indicate that with groundwater depth at 6*m*, there is possibility for liquefaction, however with lowering the groundwater level this possibility diminishes.

2. 3. 3. The Effect of Groundwater Level on Surface Dilation Variations in groundwater level and pore-water pressure are factors affecting on magnitude of surface dilation in the middle of the model. Figure 20 shows variations of surface dilation in the middle of the model against time for various groundwater levels. The results indicate that with decrease in groundwater level the surface dilation in the middle of the model decreases and minimum and maximum dilation for the case where

groundwater level is at 9*m* depth are 5*cm* and 40*cm*, respectively. In cases where the groundwater level is lower than the tunnel axis the surface dilation decreases and changes to compaction.

2. 3. 4. The Effect of Groundwater Level on Bending Moment, Shearing Force and Axial Force

Bending moment, shearing force and axial forces are affected by variation in groundwater level, pore-water pressure, existing stresses in the covering soil above the tunnel. Figures 21, 22, and 23 show the variation of bending moment, shearing force and the maximum axial force in covering soil of the tunnel against time for various groundwater levels. Figure 21 indicate that as long as the groundwater level is higher than the tunnel surface the changes in groundwater level does not have considerable effect on the maximum bending moment in covering soil of the tunnel, however the formation of the bending moment location will change. In cases where the groundwater level is at zero, 3, 6, and 9*m* the maximum bending moment occurs at 3rd second and in following seconds the bending moment fluctuations decreases. With approaching the groundwater level to 10*m* and crossing from the lower half of the tunnel, the maximum bending moment increases. With lowering the groundwater level the bending moment fluctuations increase intensively beyond 3rd seconds. The critical case is when the groundwater level is lower than the tunnel and is near to the lower elements of the tunnel.

Figure 22 indicate that for groundwater level at zero, 3*m*, and 6*m* depths the maximum shearing force variation in covering soil of the tunnel is about $10\times10^4\,Pa$ and the variation limits are between zero and $10\times10^4\,Pa$. With lowering the groundwater level to 9*m* the highest shearing force occurs at 3rd seconds and is about $17\times10^4\,Pa$ however its magnitude decreases in final seconds. At 12*m* depth where the groundwater level in direction of lower half of the tunnel, the variation in maximum shearing force in covering soil of the tunnel is similar to the above half part of the tunnel. That is about $10\times10^4\,Pa$ with variation limits of zero to $10\times10^4\,Pa$; however, the maximum shearing force occurs at 4th seconds.

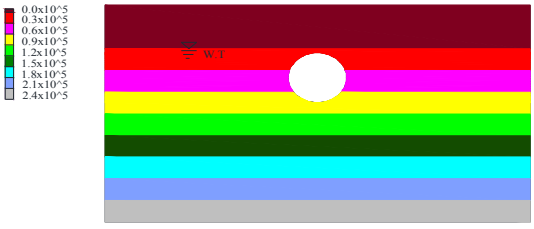

Figure 15. Pore-water pressure contour lines (for underground water level at 6*m* depth)

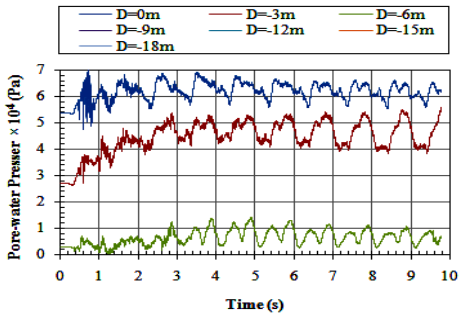

Figure 16. Pore-water pressure versus time (at 5*m* depth for groundwater level variation)

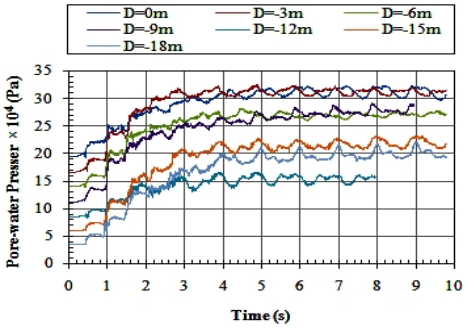

Figure 17. Pore-water pressure versus time (at 19*m* depth for groundwater level variation)

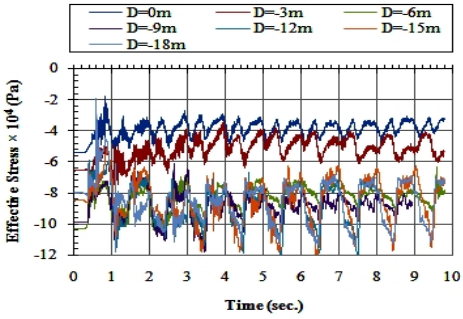

Figure 18. Effective stress versus time (at 5*m* depth for groundwater level variation)

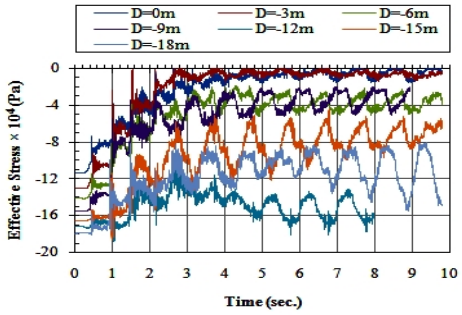

Figure 19. Effective stress versus time (at 19*m* depth for groundwater level variation)

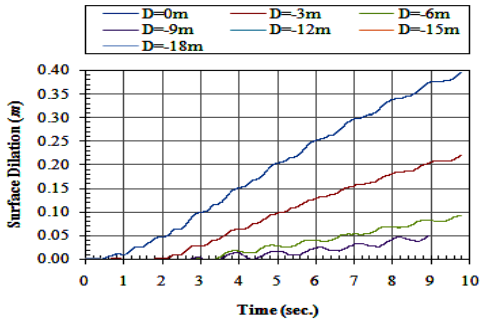

Figure 20. The surface dilation versus time (for groundwater level variation)

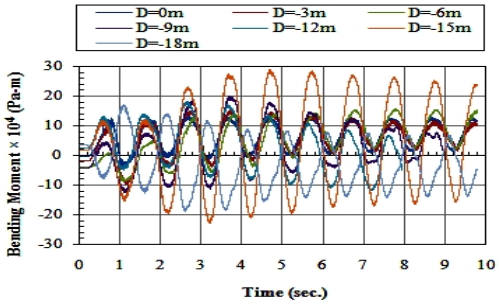

Figure 21. The bending moment versus time (for groundwater level variation)

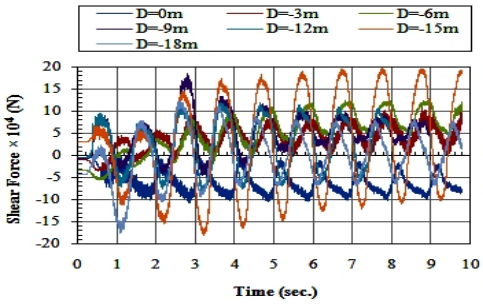

Figure 22. Shear force versus time (for groundwater level variation)

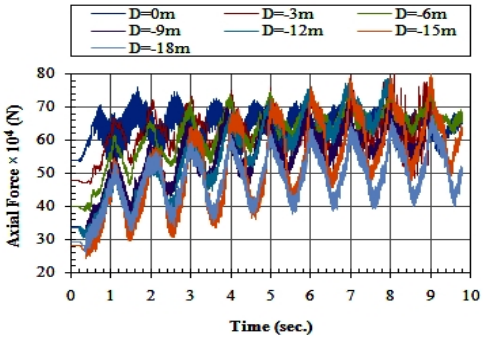

Figure 23. Axial force versus time (for groundwater level variation)

With reaching the groundwater level to 18*m* depth the maximum shearing force of almost $20\times10^4\,Pa$ is observed with fluctuation limits between $-20\times10^4\,Pa$ and $+20\times10^4\,Pa$. This contribution has similar trend with what is found for bending moment. With decreasing in groundwater level depth and crossing the critical zone, similar trends with previous parameters and concentration on shearing force at 3rd seconds are observed. Variation of axial force against time and for various groundwater levels is shown in Figure 23. The results indicate that with groundwater level at ground surface the maximum axial force of 70 *tons* is occurred at 10th seconds. With decrease in groundwater level and when reaches to 3*m* depth the axial force reaches to 80 *tons* at final seconds. With incremental decrease in groundwater level the created axial force in covering soil of the tunnel decrease and at 9*m* depth reaches to less than 70 *tons*. When the groundwater level is underneath the tunnel the created axial force reaches to its maximum magnitude. The results also show that with more decrease in groundwater level depth the axial force decrease and at 18*m* depth its magnitude reaches to 28 *tons*.

2. 4. The Effect of Porosity on Liquefaction Phenomena Porosity is an effective parameter on dry unit weight and relative density of the soil [40]. Its effects on pore-water pressure can reflect on creation of liquefaction phenomena. To investigate the effects of porosity on various parameters such as bending moments and created forces in covering soil of the tunnel, three types of Nevada soil with similar conditions, but with porosities of 0.3, 0.5, and 0.6 and various dry unit weights are selected. The variation effects of porosity on pore-water pressure, effective stress, surface heave, bending moments and created forces in covering soil of the tunnel, and intermediate elements at depths of 5*m* above and 19*m* underneath the tunnel are investigated and analyzed, respectively.

2. 4. 1. The Effect of Porosity on Pore-water Pressure Increase in porosity changes the volume of the voids of soil grain and affects on pore-water pressure. The variation of pore-water pressure against time for various porosity coefficients at 19*m* underneath and 5*m* above the tunnel are shown in Figures 24 and 25, respectively. The Nevada soil with porosity coefficient of 0.3 is selected as a base soil. The results in both Figures 24 and 25 indicate that at a constant time with increase in porosity the pore-water pressure increases.

Figure 24 indicate that at 19*m* depth underneath the tunnel the pore-water pressure reaches to a constant value at 4 seconds, while in Figure 25 and at 5*m* above the tunnel pore-water pressure has increasing trend at

the same time. This contradiction might be due to the surcharge and variation in relative density. That is the porosity of the soil above the tunnel which increases with increase in pore-water pressure and is more affected in comparison with the soil underneath of the tunnel.

2. 4. 2. The Effect of Porosity on Effective Stress With increase in porosity the dry unit weight of the soil decreases and causes variation in effective stress. Figures 26 and 27 show variation in effective stress against time at depths 5*m* and 19*m* above and underneath of the tunnel, respectively. Figure 27 indicate that at 19*m* depth with increase in porosity the effective stress is increased with time with a constant slope, while at 5*m* depth where the surcharge weight of the soil has lower effect, the effective stress is increased and reaches to zero at about 4 seconds. In other words the porosity at 5*m* depth is caused liquefaction phenomena.

2. 4. 3. The Effect of Porosity on the Surface Dilation Increase in coefficients of porosity and earthquake forces are two factors affecting the surface dilation. Figure 28 shows the variation in surface dilation against time for various coefficients of porosity. The results indicate that with increase in porosity the surface dilation decrease. The maximum surface dilation for the base model (with porosity of 0.30) is observed about 40*cm*. With increase in porosity from 0.30 to 0.60 the surface dilation reaches to its lowest value of about 12*cm*. The results also indicate that the slope variation of surface dilation against time is decreased from 40% (for porosity of 0.30) to 11.7% (for porosity of 0.60).

2. 4. 4. The Effect of Porosity on Bending Moment and Forces in Covering Soil of the Tunnel The coefficient of porosity is an effective factor in variation of bending moment and created forces in covering soil of the tunnel caused by liquefaction. Table 5 shows the bending moment, shearing force, and created axial force in the covering soil of the tunnel for various coefficients of porosity. The results indicate that with increase in coefficients of porosity from 0.3 to 0.6 the bending moment and axial force increase to 43% and 10%, respectively. However, variation in shearing force shows that with increase in coefficient of porosity up to 0.5 its value increase and then drops to a lower value.

2. 4. 5. The Effect of Porosity on Intermediate Elements The stiffness of materials used between the soil and the tunnel is generally less than concrete and more than the soil around the tunnel. Thus, the created axial and shearing forces in intermediate elements are important issues for investigations of the tunnel. Table 6 shows created shearing and normal stresses in intermediate elements between the soil and the tunnel. The results indicate that with increase in coefficients of porosity the shearing stress in intermediate elements shows increasing trend and for the models with coefficients of porosity of 0.3 and 0.6 the magnitude of shearing stresses changes from 6.8 ton/m^2 to 9.4 ton/m^2, respectively, which is almost 38% increase in shearing stresses. The results also indicate that the created normal stress in intermediate elements increase to its maximum magnitude of 52.7 ton/m^2 for the coefficient of porosity of 0.5. However, with more increase in porosity, the normal stress decrease and reaches to 51.3ton/m^2.

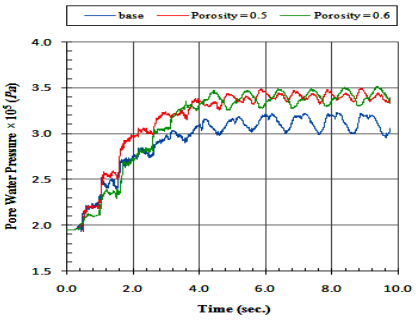

Figure 24. Pore-water pressure versus time (at ۱۹*m* beneath the tunnel)

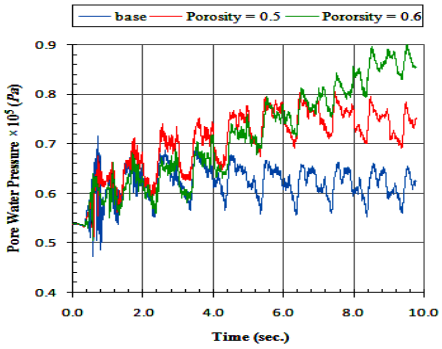

Figure 25. Pore-water pressure versus time (at ٥*m* above the tunnel)

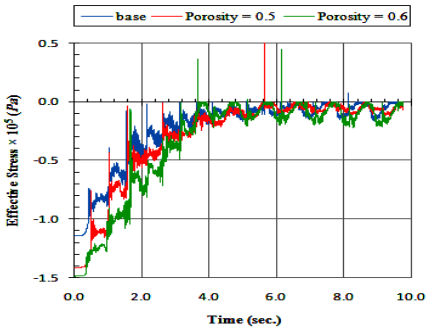

Figure 26. Effective stress versus time (at 5*m* depth for variation in porosity)

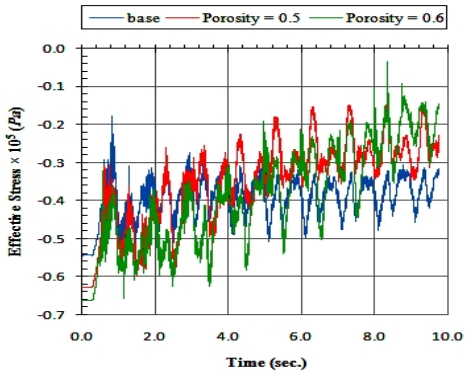

Figure 27. Effective stress versus time (at 19*m* depth for variation in porosity)

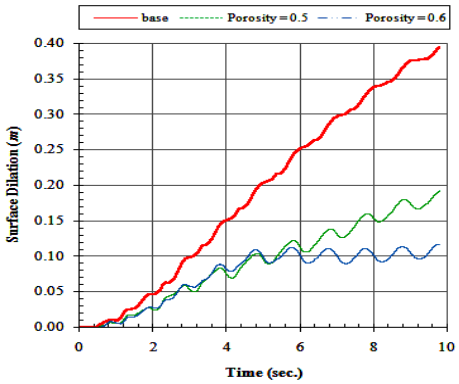

Figure 28. Surface dilation versus time (for variation in porosity)

TABLE 5. The bending moment, shearing force, and axial force created in covering soil of the tunnel

Coefficient of porosity	Maximum bending moment (*ton-m*)	Maximum shearing force (*ton*)	Maximum axial force (*ton*)
0.3	13.4	10.7	75.9
0.5	17.8	13.8	80.4
0.6	19.2	12.4	84.0

TABLE 6. Normal and shear stresses in intermediate elements between the soil and the tunnel

Coefficient of porosity	Maximum shear stress (ton/m^2)	Maximum normal stress (ton/m^2)
0.3	6.8	45.1
0.5	7.7	52.7
0.6	9.4	51.3

3. RESULTS

In the present research a tunnel is modeled in a saturated soil with liquefaction potential. For modeling of the soil and the tunnel, the square and beam elements with finite difference and FLAG software are used. The effects of liquefaction on the model with variation in parameters are investigated. Based on data and analysis performed the following results are contributed:

- ✓ Increase in water bulk modulus increased the surface dilation in the middle of the model and pore-water pressure.
- ✓ With decrease in effective stress and increase in water bulk modulus the probability of liquefaction phenomena is increased.
- ✓ The bending moment, axial and shear forces caused by liquefaction in the covering soil of the tunnel is increased with increase in water bulk modulus.
- ✓ The surface dilation in the middle of the model caused by liquefaction is decreased with decrease in groundwater level.
- ✓ In the case where groundwater level equals the lower elements of the tunnel the bending moment, shear and axial forces reach to their critical magnitudes.
- ✓ Increase in porosity causes increase in pore-water pressure underneath the underground structure and was vice versa for its upper part.
- ✓ Increase in porosity in lower depths caused decrease in effective stress of the covering soil of the tunnel, while for deeper depths was not considerable.
- ✓ The surface dilation caused by liquefaction is decreased due to increase in porosity.
- ✓ Increase in the coefficient of porosity caused increase in the bending moment, axial and shear forces in the covering soil of the tunnel.
- ✓ The normal and shear stresses of the intermediate elements are increased with increase in coefficient of porosity.

4. REFERENCES

1. Gupta, R., and Trivedi, A., "Behavior of Model Circular Footings on Silty Soils with Cellular Supports", ***International Journal of Engineering Transactions B***, Vol. 23, No. 1, (2010), 21-36.
2. Sadrnejad, S. A., "A Multi Plane Model for Natural Anisotropy of Sand", ***International Journal of Engineering Transactions B***, Vol. 16, No. 4, (2003), 311-327.

3. Hamedi Sangari, A., and Marandi, S. M., "Laboratory Studies on The Effect of Vertical Gravel Column Drains on Liquefaction Potential", ***International Journal of Engineering Transactions B***, Vol. 24, No. 3, (2011), 209-226.
4. Sadrnezad, S. A., "Multilaminate Elastoplastic Model for Granular Media", ***International Journal of Engineering****, Vol. 5 No. 1-2, (*1992), 11-24.
5. Sadenezhad S. A., "Multilaminate Elastoplastic Model for Granular Media", ***International Journal of Engineering***, Vol. 5, 1992, 11.
6. Seed, H. B., and Booker, J. R., "Stabilization of Potentially Liquefiable Sand Deposits**",** ***Journal of Geotechnical division***, Vol. 103, No. 7, (1977), 757-768.
7. Casagrande, A., "Liquefaction and Cyclic Deformation of Sand-A critical review", ***5th Pan American Conference on Soil Mechanics and Foundation Engineering***, Buenos Aires, Argentina, (1975).
8. Wang, W. L., Wang, T. T., Su, J. J., Lin, CH., Seng, C. R., and Huang, T. H., "Assessment of Damage in Mountain Tunnels due to the Taiwan Chi-Chi Earthquake", ***Tunneling and Underground Space Technology***, (2001), Vol. 16, 133-50.
9. Yegian, M. K., Ghahraman, V. G., Nogole-Sadat, M. A. A., and Daraie, H., "Liquefaction during the 1990 Manjil earthquake", Iran: Case history data, ***Seismological Society of America*****,** Vol. 85, No. 1, (1995), 66–82,.
10. Matsumuto, J., "Sanitary Facilities", General Report on the Niigata Earthquake of 1964. *Tokyo Electrical Engineering College Press*, (1968).
11. Tohoku, B., and Nihonkai, C., *Japanese Society of Soil Mechanics Foundation Engineering*, "Report on the Damage Investigation of the 1983 Nihonkai-Chubu Earthquake" (in Japanese), (1983).
12. Koseki, J., Matsuo, O., Ninomiya, Y., and Yoshida, T., "Uplift of Serer Manholes during the 1993 Kushiro-oki Earthquake", 109-21, S.L.: *Soils Foundation*, Vol. 37, (1997).
13. Tokimatsu, K., Suzuki, Y., and Tamura, S. "Preliminary Report on the Geotechnical Aspects of 1993 Hokkaido Nansie-oki Earthquake", New Delhi: ***13th International Conference on Soil Mechanics and Foundations Engineering***, (1994).
14. Hall, W. J., And O'Rourke, T. D., "Seismic Behavior and Vulnerability of Pipelines", *Proc. 3 U.S. Conf.*, Lifeline Earthquake: S.N. 761-73, (1991).
15. Mir Mohammad Hosseini, S. M., and Moghaddas Tafreshi, S. N., "Soil-Structure Interaction of Buried Pipes under Cyclic Loading Conditions", ***International Journal of Engineering Transactions B*:**, Vol. 15, No. 2, (2002), 117-124.
16. Ghodrati Amiri, G., Mahmoodi, H. and Razavian Amrei, S. A., "Probabilistic Seismic Hazard Assessment of Tehran Based on Arias Intensity", ***International Journal of Engineering Transactions B***, Vol. 23, No. 1, (2010), 1-20.
17. Shimamara, K., et al., "Loads on Pipes Buried in a Non-Liquefaction Layer Due to Liquefaction -Induced Ground Displacement", *Proc. of the 12th World Conf. on Earthquake Eng.,* Rocketbyte Information System: Aucland, New Zealand, (2000), 492-499.
18. Mohri, Y., Kawabata, T., and Ling, H. I., "Experimental Study on the Effects of Vertical Shaking on the Behavior of Underground Pipelines", ***Proc. of the 2nd Int. Conf. on Earthquake Geotechnical Engineering,*** **Ed**. Pedro. S.Seco e Pinto, Balkema: Retterdom, (1999), 489-494.
19. Mir Mohammad Hosseini, S. M. and Moghaddas Tafreshi, S. N., "A New Physical Model to Study the Behavior of Buried Pipes Under Cyclic Loading Condition", ***Proc. of the 12th World Conf. on Earthquake Eng.,*** Rocketbyte Information System: Auckland New Zealand, P. No. 0889, (2000), 889-896.
20. Tajimi M., "Damage Done by the Great Earthquake Disaster of the Hanshin-Awaji District to the Kobe Municipal Subway System and Restoration Works of The Damage". Japan Railway Eng., Vol. 137, (1996), 19–23.
21. O'Rourke, T. D., Goh, S. H., Menkiti, C. O., and Mair, R. J., "Highway Tunnel Performance during the 1999 Duzce Earthquake", ***15th International Conference on Soil Mechanics*** *and* ***Geotechnical Engineering***, (2001).
22. Wang, J.M., "Distribution of Earthquake Damage to Underground Facilities during the 1976 Tang-shan Earthquake", ***Earthquake Spectra***, Vols. 1-4, (1985).
23. Schmidt, B., and Hashash, Y. ST., "U.S. Immersed Tube Retrofit Tunnels**",** ***Tunneling and Underground Space Technology***, Vol. 30, No. 11, (1998), 22-4.
24. Azadi, M. and Mir Mohammad Hoessini, S. M., "Investigate of Effect of Liquefaction on Shield Tunnel**",** ***Tehran, SEE5***, (2007).
25. Chou, H., Yang, C., Hsieh, B., and Chang, S., "A Study of Liquefaction Related Damages on Shield Tunnels", ***Tunneling and Underground Space Technology,*** 16, (2001), 185-193.
26. Khoshnoudian, F., "Etude du Comortement des Tunnels Sous Chargement Sismique", Ph.D. Thesis, France, University of Sciences and Technologies of Lille, (1999).
27. Khoshnoudian, F. and Shahrour, I., "Numerical Analysis of the Seismic Behavior of Tunnels Constructed in Liquefiable Soils", ***Soils and Foundation***, Vol. 42, (2002).
28. Liu, H., and Song, E., "Seismic Response of Large Underground Structures in Liquefiable Soils Subjected to Horizontal and Vertical Earthquake Excitations", ***Computers and Geotechnics***, Vol. 32, (2005).
29. Liu, Huabei, and Song, Erxiang, "Working Mechanism of Cutoff Walls in Reducing Uplift of Large Underground Structures Induced by Soil Liquefaction", ***Computers and Geotechnics***, Vol. 33, (2006), 209-221.
30. Azadi, M., "Effect of Soil Liquefaction on Shield Tunnels", *Ph.D. Thesis*, Civil Eng. Department, Faculty of Amirkabir University of Technology, Iran, (2008).
31. Azadi, M., and Mir Mohammad Hoessini, S. M., "The Uplifting Behavior of Shallow Tunnels within the Liquefiable Soils under Cyclic Loadings", ***Tunneling and Underground Space Technology***, (2009).
32. Azadi, M., and Mir Mohammad Hosseini, S. M., "Analyses of the Effect of Seismic Behavior of Shallow Tunnels in Liquefiable Grounds", ***Tunneling and Underground Space Technology***, 2010.
33. Tokida, K., and Ninomiya, Y., "Experimental Study of the Uplift Deformation of Underground Structure Induced by Soil Liquefaction", ***Japan National Center for Earthquake Engineering Research, Proceedings from the 4th Japan-U.S.,*** (1992).
34. Bahadori, A., and Hari, V., "Prediction of Bulk Modulus and Volumetric Expansion Coefficient of Water for Leak Tightness Test of Pipelines", ***International Journal of Pressure Vessels and Piping***, Vol. 86, (2009).
35. Cundall et al. "Fast Lagrangian Analysis of Continua Manual", *Online Manual*, (2001).
36. Koohi S., "Modeling and Numerical Analysis of Lateral Spreading Due to Liquefaction", ***M.Sc. dissertation, Amirkabir university of Tehran***, (2004).
37. Abbas Sorush and Sheila Koohi, "Numerical Analysis of Liquefaction-Induced Lateral Spreading", ***13th World Conference on Earthquake Engineering, Vancouver, B.C., Canada,*** (2004), 1-6.

38. Martin, G. R, Finn, W. D, and Seed, H. B., "Fundamentals of Liquefaction under Cyclic Loading", *Geotech, Div, ASCE*, 101(GTS), (1975).

39. Cundall, P. A., H. Hansteen, S. Lacasse and P. B. Selnes, "NESSI - Soil Structure Interaction Program for Dynamic and Static Problems", ***Norwegian Geotechnical Institute***, (1980), 51508-9.

40. Das, B. M., "Advanced Soil Mechanics", ***Elsevier Science***, New York, (1990).

Parametric Study of the Covering Soil of Tunnels Constructed in Liquefiable Soil

S. M. Marandi, A .R. Rasti

Department of Civil Engineering, Shahid Bahonar University, Kerman, Iran

P A P E R I N F O

Paper history:
Received 31 May 2012
Received in revised form 5 August 2012
Accepted 30 August 2012

Keywords:
Liquefaction
Tunnel
Water Bulk Modulus
Porosity
Groundwater Level

چکیده

خرابی های ناشی از زلزله پیوسته یکی از دغدغه های مهندسین راه و ساختمان بوده و در علم ژئوتکنیک روانگرائی از مهمترین پدیده های ناشی از زلزله میباشد. این پدیده در اثر افزایش فشار آب منفذی ناشی از زلزله، صفر شدن تنش مؤثر و از بین رفتن مقاومت برشی خاک بوجود می آید و موجب تخریب سازه های ساخته شده در زیر و روی سطح زمین میگردد. درصورت ساخت سازه های زیرزمینی و یا تونل های عبور کرده از میان خاکهای سست تراکم پذیر، با افزایش نیروها و لنگرهای اطراف سازه که به روانگرائی منجر میگردد ممکن است صدماتی به خاکها و سازه های اطراف آن وارد نماید. در این مقاله تونل عبور کرده از میان خاک با پتانسیل روانگرائی مدل گردیده و پس از تعادل استاتیکی ار لحاظ دینامیکی مورد تجزیه و تحلیل قرار گرفته است. با مدلسازی روانگرائی و اندازه گیری نیروها و لنگرهای ایجاد شده در خاک اطراف تونل، پارامترهائی مثل مدول توده آب، سطح آب زیرزمینی و ضریب پوکی خاک مورد ارزیابی قرار گرفته است. نتایج این تحقیق نشانداده است که پارامترهای مذکور تاثیر بسزائی در تغییرات تنش مؤثر، لنگرها و نیروهای ایجاد شده، و اتساع سطحی خاک اطراف تونل دارد.

doi: *10.5829/idosi.ije.2012.25.04a.05*